Nodule-specific Cu^+-chaperone NCC1 is required for symbiotic nitrogen fixation in *Medicago truncatula* root nodules

Cristina Navarro-Gómez[1], Javier León-Mediavilla[1], Hendrik Küpper[2,3], Mario Rodríguez-Simón[1], Alba Paganelli-López[1,4], Jiangqi Wen[5], Stefan Burén[1,4], Kirankumar S. Mysore[5], Syed Nadeem Hussain Bokhari[2], Juan Imperial[1], Viviana Escudero[1,*], Manuel González-Guerrero[1,4,*]

[1]Centro de Biotecnología y Genómica de Plantas. Universidad Politécnica de Madrid (UPM)- Instituto Nacional de Investigación y Tecnología Agraria y Alimentaria (INIA/CSIC). Campus de Montegancedo UPM. 28223 Pozuelo de Alarcón. Spain.

[2]Lab. Plant Biophysics and Biochemistry. Institute of Plant Molecular Biology. Biology Centre. Czech Academy of Sciences. Biology Centre. České Budějovice. Czech Republic.

[3]Dept. Experimental Plant Biology. Faculty of Sciences. University of South Bohemia. České Budějovice. Czech Republic.

[4]Dept. of Biotechnology-Plant Biology. Escuela Técnica Superior de Ingeniería Agraria, Alimentaria y de Biosistemas. Universidad Politécnica de Madrid. 28040 Madrid. Spain.

[5]Institute for Agricultural Biosciences. Oklahoma State University. Ardmore OK73401. USA.

* Corresponding authors: Manuel González-Guerrero (manuel.gonzalez@upm.es)
Viviana Escudero (viviana.escudero@upm.es)

Running title: NCC1 is required for symbiotic nitrogen fixation

ABSTRACT

Cu^+-chaperones are a diverse group of proteins that allocate Cu^+ ions to specific copper-proteins, creating different copper pools targeted to specific physiological processes. Symbiotic nitrogen fixation carried out in legume root nodules indirectly requires relatively large amounts of copper e.g. for energy delivery via respiration, for which targeted copper deliver systems would be required. MtNCC1 is a nodule-specific Cu^+-chaperone encoded in the *Medicago truncatula* genome, with a N-terminus Atx1-like domain that can bind Cu^+ with picomolar affinities. This gene is expressed primarily from the late infection zone to the early fixation zone, and is located in the cytosol, associated to plasma and symbiosome membranes, and within nuclei. Consistent with its key role in nitrogen fixation, *ncc1* mutants have a severe reduction of nitrogenase activity, and a 50% reduction in copper-dependent cytochrome *c* oxidase activity. A subset of the copper-proteome is also affected in the mutant nodules. Many of these proteins can be pulled-down when using a Cu^+-loaded N-terminal MtNCC1 moiety as a bait, indicating a role in nodule copper homeostasis and in copper-dependent physiological processes. Overall, these data suggest a pleiotropic role of MtNCC1 in copper delivery for symbiotic nitrogen fixation.

Keywords: copper, nitrogen fixation, metallochaperone, nodulation

INTRODUCTION

Copper is an essential nutrient for plants (Marschner and Marschner, 2011). It is involved in key physiological processes such as photosynthesis, respiration, ethylene signalling, or free radical control, among many others (Andresen et al, 2018). This versatile use of copper is largely based on its ability to transition between two redox states (Cu^{+} and Cu^{2+}) in physiological conditions (Burkhead et al., 2009). However, that same property makes copper a toxic reagent at slightly higher concentration (Küpper and Andresen, 2016). One suggested mechanism of toxicity is the non-enzymatic catalysis of Fenton-style reactions producing damaging free radicals (Goldstein et al., 1993). Furthermore, excess copper can displace other essential transition metals from the active site of metalloproteins (Küpper et al., 1996; Küpper et al., 2002; Macomber and Imlay, 2009). As a result, and to prevent copper damage to the cell structures, the "free", hydrated, concentrations of copper in the cytosol are maintained at extremely low levels, less than one ion per cell (Changella, 2003). This is achieved by the coordinated action of small, copper-binding molecules, as well as proteins known as Cu^{+}-chaperones (Robinson and Winge, 2010; Flis et al., 2016).

The role of Cu^{+}-chaperones is to deliver copper to different copper-proteins, protecting the cell from copper toxicity (Lin et al., 1997; Wong et al., 2000). Cu^{+}-chaperones bind Cu^{+} with picomolar (pM)- femtomolar (fM) affinity (Rae et al., 1999; Palumaa et al., 2004), which prevents unspecific copper release prior to docking with a compatible protein. This means that metalation is not simply the result of relative copper-binding affinities, but also of the specific protein-protein interaction between donor and acceptor proteins. Consequently, different copper pools are created based on the ability of each protein to interact and exchange copper with one or another Cu^{+}-chaperone. *Saccharomyces cerevisiae* has at least three of these pools: the secretory pathway that receives copper from Atx1 (Lin et al., 1997); the mitochondria that obtain copper from COX17 (Palumaa et al., 2004); and the Cu, Zn superoxide dismutase that gets it from CCS (Rae et al., 1999). Multicellular organisms are expected to have a larger number of such proteins, which are related in structure but serve a diversity of functions. Plants have at least a CCS orthologue (Chu et al., 2005), two Cu^{+}-chaperones driving copper to mitochondria (Attallah et al., 2011), another in the stroma (Blaby-Haas et al., 2014), and three ATX1 orthologues with the characteristic Cu^{+}-binding CXXC motive: ATX1 (Shin et al., 2012), CCP (Chai et al., 2020) and CCH (Mira et al., 2001), the later with a C-terminal domain of unknown function. This multiplicity of Cu^{+}-chaperones hints not only

103 at the existence of different copper pools, but also at their specialized roles in plant
104 physiology. For instance, ATX1 seems to be involved in buffering through copper
105 deficiency or excess (Shin et al., 2012), CCH has been proposed to be involved in
106 recovering copper during leave senescence (Mira et al., 2001), and CCP plays a role in
107 plant immunity (Chai et al., 2020). Therefore, it should be expected that other, new Cu^+-
108 chaperones are associated with other copper-dependent processes.

109 While leaves are the main copper sink in most plants during vegetative growth,
110 legumes have a second, major copper sink in their root nodules (Johnston et al., 2001;
111 Senovilla et al., 2018). After the exchange of specific signals between legumes and a
112 group of bacteria known as rhizobia, cells in the root cortex, pericycle and endodermis
113 proliferate to produce nodules (Downie, 2014; Xiao et al., 2014). Concomitant to nodule
114 development, rhizobia penetrate and colonize nodule cells. Surrounded by the plant-
115 derived symbiosome membrane, rhizobia differentiate into bacteroids that synthesize
116 nitrogenase to fix nitrogen. This developmental process can be easily followed in
117 indeterminate-type nodules, such as those in pea or in *Medicago truncatula*.
118 Indeterminate nodules maintain their apical meristem over time, leading to a spatial-
119 temporal gradient. As a result, four developmental zones can be observed in these
120 nodules: the apical meristem (zone I), the infection-differentiation zone (zone II), an
121 interzone where oxygen levels drop to prevent nitrogenase inhibition, so that nitrogen
122 fixation can occur in the fixation zone of the nodule (zone III), and a senescent zone (zone
123 IV) in older nodules (Vasse et al., 1990). In exchange for this fixed nitrogen, the host
124 plant provides photosynthates and mineral nutrients, including copper (Udvardi and
125 Poole, 2013; Senovilla et al., 2018).

126 Legume nodules accumulate high levels of copper (around 50 μg/g) (Senovilla et
127 al., 2018), evidencing an important role for this nutrient in nodule development and/or
128 symbiotic nitrogen fixation. Further evidence is provided by the existence of a nodule-
129 specific copper uptake transporter, MtCOPT1, that is required for optimal nitrogen
130 fixation and cytochrome oxidase activity of bacteroids (Senovilla et al., 2018). Therefore,
131 it should be expected that specific mechanisms are in place to ensure copper allocation to
132 enzymes involved in symbiotic nitrogen fixation in legume nodules, and that this is
133 achieved via dedicated Cu^+-chaperones. This manuscript provides data supporting this
134 hypothesis, as it reports that *Medtr3g067750* is a nodule-specific Cu^+-chaperone (NCC)
135 that is essential for symbiotic nitrogen fixation.
136

137 **RESULTS**

138 **MtNCC1 is a Cu^+-chaperone**

139 To identify candidate Cu^+-chaperones in *Arabidopsis thaliana* and *M. truncatula*,
140 we collected those sequences annotated as such, as well as those annotated as metal-
141 binding domain proteins or HIPP, removing those that did not contain a CXXC Cu^+-
142 binding motive. Over 30 different candidates were identified in the genomes of these two
143 plant species (Fig. S1). Within *M. truncatula*, there was a nodule-specific candidate,
144 *Medtr3g067750* (NCC1, for Nodule-specific Cu^+-Chaperone1), as indicated by the
145 available transcriptomic databases (Fig. S2). This expression pattern was validated by
146 qRT-PCR analyses (Fig. 1A). Protein modelling showed the existence of two different
147 protein domains: a N-terminal Atx1-like domain comprised by the first 78 amino acids
148 ($MtNCC1_{1-78}$) that included the CXXC motif, and a C-terminal, intrinsically disordered
149 region, with an E-rich motif (Fig. 1B).

150 Yeast complementation assays of the yeast *atx1* mutant were used to determine
151 whether the candidate protein above could function as a Cu^+-chaperone. This strain
152 cannot grow in non-fermentative carbon sources. However, *atx1* showed wild-type
153 growth when expressing *MtNCC1* or $MtNCC1_{1-78}$ (Fig. 1C). To further determine whether
154 MtNCC1 could work as a Cu^+-chaperone, Strep-tagged $MtNCC1_{1-78}$ was purified from
155 *Escherichia coli* (Fig. S3) and used to determine Cu^+-binding stoichiometry and affinity.
156 As expected from an Atx1-like chaperone, $MtNCC1_{1-78}$ bound one Cu^+ per molecule with
157 an affinity constant of 2.45 pM^{-1} (Fig. 1D). A similar stoichiometry was observed after
158 incubating $MtNCC1_{1-78}$ with a 10-fold molar excess of Cu^+ and removing the unbound
159 metal (Fig. S4).

160

161 **MtNCC1 is located in the cytosol and nucleus of nodule cells**

162 To determine whether MtNCC1 was produced in the nodule, promoter-GUS
163 fusions were transformed in *M. truncatula* plants. As shown in Fig 2A, *MtNCC1* was
164 highly expressed in the infection-differentiation zone (ZII), interzone (IZ) and early
165 fixation zone (ZIII) of the nodules, although lower expression levels could be found in
166 older fixation zone areas. This expression pattern is consistent with the transcriptomic
167 data obtained from laser-captured micro-dissected cells in the Symbimics database (Fig.
168 2B). Moreover, immunolocalization of hemagglutinin epitope (HA)-tagged MtNCC1
169 showed a similar distribution (Fig 2C). Higher magnification images of nodule cells
170 showed MtNCC1-HA in the cytoplasm and in the nuclei in infected and uninfected cells

171 (Fig. 2D). This distribution pattern was not observed in un-transformed plants (Fig. S5).
172 Additionally, MtNCC1$_{1-78}$-HA had the same distribution pattern (Fig. S6). Electron-
173 microscopy images using a gold-conjugated antibody revealed that MtNCC1-HA was
174 found in the cytosol, as well as associated with the plasma and symbiosome membranes
175 (Fig. 2E).
176
177 **MtNCC1 is required symbiotic nitrogen fixation**
178 To determine the physiological role of MtNCC1, an insertional *ncc1* mutant was
179 obtained from a *M. truncatula Tnt1* mutant collection. This line had an insertion in
180 position +1044 that led to loss of *MtNCC1* expression (Fig. 3A). As expected, the mutant
181 line did not present any apparent phenotype under non-symbiotic conditions (Fig S7), but
182 showed a significantly reduced growth and biomass production in symbiosis (Fig. 3B,C).
183 No significant changes in nodule development were observed compared to wild-type
184 plants (Fig. S8). The nitrogenase activity in *ncc1* plants was severely reduced (Fig. 3D).
185 Analyses of *MtNCC1* wild-type *ncc1* segregants suggested that no additional *Tnt1*
186 insertions elsewhere in the genome could explain these phenotypical effects (Fig. S9).
187 Furthermore, growth and nitrogenase activity were restored by introducing a wild-type
188 copy of *MtNCC1* into the mutant line (Fig 3B-D). Finally, cytochrome oxidase activity
189 was significantly reduced in bacteroids, but to a much lower extent than the nitrogenase
190 activity (Fig. 3E).
191
192 ***MtNCC1* mutation affects a subset of the copper-proteome**
193 Consistent with the role of MtNCC1 in copper metabolism, increasing copper
194 concentrations by 10-fold in the nutrient solution was sufficient to restore wild-type
195 growth and nitrogenase activity in *ncc1* plants (Fig. 4). However, overall copper content
196 in the analysed plant organs (roots, shoots, and nodules) was not significantly altered in
197 *ncc1* plants (Fig 5A). Iron levels were not affected either (Fig. 5B). Importantly,
198 metalloproteomic analyses on nodule soluble protein extracts from wild-type and *ncc1*
199 nodules showed reduced copper contents in a subset of the proteome (Fig. 6A). The
200 largest differences were found around 110 kDa and 60 kDa. As this was a separation only
201 by SEC, the copper proteins only represented a small proportion of the total proteins
202 eluting during the times when a maximal difference between the wild-type and *ncc1*
203 samples was observed. This becomes clear when looking at the profiles of other metals

204 at the same time and comparing the UV/VIS spectra with the metal chromatograms
205 (regions of interest in Figures 6B, 6C, complete time range in Figure S10).
206 Therefore, although copper-binding proteins were affected, the total number of proteins
207 contained in two fractions (chosen in the MW ranges of max. differences in copper,
208 Fig 6A) in wild type and *ncc1* nodules remained largely the same (Tables S1 and S2);
209 only 70 out of 1529 proteins in fraction 1 and 12 out of 1900 proteins in fraction 2 missing
210 in *ncc1* compared to wild type. None of the ten most abundant of these differentially
211 expressed proteins have a known role in copper-homeostasis (Table 1). Looking at the
212 entire HPLC-ICPsfMS chromatograms in more detail, (Fig S10) reveals additional
213 changes in the metalloproteome that would result from the cross-talk between copper
214 homeostasis and that of other elements. Analysing these changes would be a topic for
215 another study.
216 In a further attempt to identify proteins that would accept Cu^+ by interacting with
217 MtNCC1, Cu^+-loaded $MtNCC1_{1-78}$ ($MtNCC1_{1-78}\cdot Cu^+$) was used as a bait for pull-down
218 assays. In order to ensure that the identified proteins were those that specifically
219 interacted with $MtNCC1_{1-78}\cdot Cu^+$ and not with the resin, control pull-down assays in which
220 no bait was bound to the resin were done in parallel. The proteins specifically retained by
221 $MtNCC1_{1-78}\cdot Cu^+$ are indicated in Table S3. Approximately, one third of these proteins
222 were also present in the selected fractions from the metalloproteomic analyses (Table S4),
223 and mostly they are putatively involved in D-gluconate catabolism, S-adenosylmethione
224 (SAM) cycle, endoplasmatic reticulum unfolded protein response, and protein import into
225 the nucleus. To further confirm some of these interactions, Bi-molecular Fluorescence
226 Complementation (BiFC) studies were carried out in agroinfiltrated tobacco leaves
227 expressing *MtNCC1*$_{1-78}$ together with selected candidates identified in the pull-down
228 experiments. As shown in Fig. 7, $MtNCC1_{1-78}$ interacted with thioredoxin-dependent
229 peroxiredoxin (*Medtr7g105830)*, SAM synthase (*Medtr2g046710),* putative universal
230 stress protein (*Medtr1g088640)*, and pathogenesis-related protein (*Medtr2g076010)*. No
231 signal was observed when $MtNCC1_{1-78}$ was expressed in leaves infiltrated with the empty
232 vectors (Fig. S11).
233
234 **DISCUSSION**
235 Symbiotic nitrogen fixation in legume root nodules is a process that requires of a
236 large transfer of transition elements from the host plant to the root nodules (O'Hara, 2001;
237 González-Guerrero et al., 2016). In recent years, many of the transporters mediating this

238 transfer have been identified (Tejada-Jiménez et al., 2015; Abreu et al., 2017; Tejada-
239 Jiménez et al., 2017; Senovilla et al., 2018; Castro-Rodríguez et al., 2020; Escudero et
240 al., 2020), as well as metal-chelating molecules that maintain metal solubility in saps and
241 apoplast (Kryvoruchko et al., 2018; Escudero et al., 2020b). In the case of copper, there
242 is a high degree of specificity in nodules. Host plants, such as *M. truncatula*, express a
243 nodule-specific Cu^+-uptake transporter, MtCOPT1, to ensure copper uptake by infected
244 cells (Senovilla et al., 2018). Bacteroids also synthesize nodule-specific copper
245 transporters, such as FixI, a P_{1B}-ATPase responsible for providing copper for a nodule-
246 specific high-affinity cytochrome oxidase (Kahn et al., 1989; Preisig et al., 1996).
247 However, an additional level of control based on Cu^+-chaperones must exist so that
248 copper is specifically delivered from very few copper transporters to multiple different
249 copper-enzymes. We have identified MtNCC1 as a representative of this layer of control.
250 The relationship of MtCOPT1 and MtNCC1 roles in nodule copper homeostasis is
251 suggested by the presence of both proteins in the same nodule zones (mainly from late
252 infection to early fixation zones). This hints at a functional pairing between the two
253 proteins, *i.e.* the transporter transfers copper to the chaperone. Moreover, MtNCC1 is not
254 the only copper delivery system to bacteroids. As for *copt1-1*, copper fortification of the
255 nutrient solution is sufficient to restore wild-type growth and nitrogenase activity,
256 suggesting that MtNCC1 is only necessary below a certain copper concentration threshold
257 and that other lower-affinity system(s) can functionally complement MtNCC1.
258 The connection between the reduction of nitrogenase activity and mutation of
259 *MtNCC1* is not direct. Nitrogenase does not use copper as a cofactor, nor is copper known
260 to be directly needed for its synthesis (Burén et al., 2020). In previous studies (Senovilla
261 et al., 2018), reduction of nitrogenase activity could be explained as the consequence of
262 the reduction of cytochrome oxidase activity that would limit the energy available to
263 bacteroids. However, the partial reduction in cytochrome oxidase activity cannot explain
264 the drastic loss of nitrogenase activity in *ncc1*. The explanation cannot be altered nodule
265 morphology either (wild-type and *ncc1* nodules do not seem different), nor can it be a
266 collateral effect on iron metabolism in the nodule. The reason must instead lie in the
267 subset of proteins that interact with MtNCC1. Many of them, when forming complexes
268 with $MtNCC1_{1-78}$ can be detected in the nuclei. Some of them could be involved in
269 epigenetic regulation (SAM synthases) (Liu et al., 2020), in the response to plant-microbe
270 interactions (pathogenesis-related proteins) (Kaur et al., 2017), or in the coordination
271 between host and bacteroid (Nodule-specific Cysteine-rich peptides, NCRs) (Maróti et

272 al., 2015), but their specific roles in symbiotic nitrogen fixation still remain to be
273 determined. Our metalloproteomic and pull-down assays have unveiled a number of new
274 putative copper-proteins that have to be further validated biochemically and in the context
275 of symbiotic nitrogen fixation. Other candidate copper-proteins might emerge from
276 studying the interaction with the C-terminal domain of MtNCC1. However, all our efforts
277 in that direction were fruitless because of our failure to recover either full MtNCC1 or C-
278 domain MtNCC1 from the inclusion bodies that formed when they were expressed in *E.*
279 *coli.*

280 Interestingly, MtNCC1 is not only located in the cytosol or in the proximity of the
281 membranes, it can also be detected in nuclei, as was the case of CCP in Arabidopsis (Chai
282 et al., 2020). However, no nuclear localization signal could be found in the MtNCC1
283 sequence. Alternatively, the observed nuclear localization could be the result of
284 interactions with other proteins. BiFC studies indicate that this is the case, as only some
285 of the interactions tested led to $MtNCC_{1-78}$ detection in nuclei. The migration of MtNCC1
286 from cytosol to nucleus will be likely facilitated by importins (Merkle, 2011), some of
287 which have been detected in the pull-down assays. The physiological relevance of this
288 localization is not evident. Theoretically, copper could be delivered to any proteins in the
289 cytosol and then the newly-metallated proteins could migrate to the nucleus. It could be
290 argued that copper transfer to the nucleus could be conditional to specific environmental
291 cues, or that some sort of ternary complex in the nucleus would be needed. These
292 possibilities will have to be specifically tested in the future. However, one role that
293 nuclear MtNCC1 does not seem to play is to deliver Cu^+ to a putative copper sensor. The
294 existence of a nodule-specific copper sensor can be inferred from the previous work on
295 MtCOPT1. Lack of copper uptake by nitrogen-fixing cells did not result in nodules
296 containing less copper, but the opposite (Senovilla et al., 2018). This was interpreted as a
297 copper-deficiency signal being sent from nodule cells, that led to more copper being
298 delivered. However, since MtCOPT1 was not present, this copper did not reach the cell
299 cytosol and accumulated in the apoplast. This phenotype, however, was not observed in
300 *ncc1* mutants, in which no significant change in copper contents was observed.

301 In summary, in this work we have shown the existence of a nodule-specific Cu^+-
302 chaperone that is required for nitrogen fixation. We have identified changes in the nodule
303 copper-proteome as a result of losing MtNCC1 activity, as well a new putative copper-
304 proteins that might play a role in symbiotic nitrogen fixation. Future work will be directed

305 to determining the physiological role of these proteins and to verifying that they can
306 accept copper from MtNCC1.
307
308 **METHODS**
309 **Biological materials and growth conditions**
310 *Medicago truncatula* Gaertner R108 seeds were scarified in pure H_2SO_4 for
311 7.5 min. Then, they were washed with cold water and sterilized with 50% bleach for
312 1.5 min and imbibed in sterile water in darkness overnight. On the following day, seeds
313 were placed on water-agar plates for 48 h at 4°C, and then allowed to germinate at 22°C
314 for 24 h. Seedlings were planted in sterile perlite pots and inoculated with *Sinorhizobium*
315 *meliloti* 2011 or *S. meliloti* 2011 transformed with pHC60 (Cheng and Walker, 1998), as
316 indicated. Plants were grown in a greenhouse in 16 h light/8 h dark and 22°C and watered
317 with Jenner's solution or water every 2 d, alternatively (Brito et al., 1994). Nodules were
318 collected at 28 days-post-inoculation (dpi). Non-inoculated plants were cultivated in
319 similar conditions, but they were watered every 2 weeks with Jenner's solution
320 supplemented with 2 mM NH_4NO_3. For hairy-root transformations, *M. truncatula*
321 seedlings were infected with *Agrobacterium rhizogenes* ARqua1 carrying the appropriate
322 binary vector as described (Boisson-Dernier et al., 2001). In agroinfiltration experiments,
323 *Nicotiana benthamiana* (tobacco) leaves were infected with the plasmid constructs in
324 *A. tumefaciens* GV3101 (Deblaere et al., 1985). Tobacco plants were grown under the
325 same conditions as *M. truncatula*.
326 For yeast complementation assays, *Saccharomyces cerevisiae* strain Δ*atx1* and its
327 parental strain BY4741 (MATa *his3Δ 1 leu2Δ 0 met15Δ 0 ura3Δ 0*) were purchased from
328 the Yeast Knockout Collection (GE Dharmacon). Yeasts were grown in yeast peptone
329 dextrose (YPD) or in synthetic dextrose (SD) media supplemented with 2% glucose
330 (Sherman et al., 1983). Phenotypic characterization was performed in yeast peptone
331 ethanol glycerol (YPEG) medium (Li & Kaplan, 2001).
332 For protein purification, *Escherichia coli* BL21 (DE3) pLysS (Wood, 1966) (*E.*
333 *coli* str. B F–*ompT gal dcm lon hsdSB* ($r_{B-}m_{B-}$) λ(DE3 [*lacI lacUV5-T7p07 ind1 sam7*
334 *nin5*]) [$malB^+$]$_{K-12}$ (λ^S) pLysS [T7p20 ori_{p15A}](Cm^R) was used to produce the required
335 amount of protein.
336

337 **Quantitative real-time RT-PCR**

338 RNA isolation and cDNA synthesis were carried out as previously described
339 (Tejada-Jiménez et al., 2015). Gene expression was studied by quantitative real-time RT-
340 PCR (9700, Applied Biosystems) with primers indicated in Table S5 and normalized to
341 the *M. truncatula Ubiquitin carboxy-terminal hydrolase* gene (*Medtr4g077320*). Real-
342 time cycler conditions have been previously described (González-Guerrero et al., 2010).
343 Determinations were performed with RNA extracted from three independent biological
344 samples, with the threshold cycle determined in triplicate. The relative levels of
345 transcription were determined with the $2^{-\Delta Ct}$ method.

346

347 **Yeast complementation assays**

348 *MtNCC1* and *MtNCC1*$_{1\text{-}78}$ cDNAs were cloned into the yeast expression vector
349 pDR196, between PstI and XhoI restriction sites, by homologous recombination in yeast
350 (primers indicated in Table S5). For yeast transformation, a lithium acetate-based method
351 was used as described (Schiestl and Gietz, 1989). Transformants were selected in SD
352 medium by uracil autotrophy. Phenotypic analysis of yeast transformants were done on
353 YPEG plates (Li & Kaplan, 2001).

354

355 **Protein Expression and Purification.**

356 *MtNCC1*$_{1\text{-}78}$ was obtained by PCR using *MtNCC1* cDNA as the template (primers
357 indicated in Table S5). The resulting cDNA was cloned between *NdeI* and *BamHI*
358 restriction sites in a modified version of pET16b (courtesy of Dr. Luis Rubio). This
359 plasmid adds two N-terminal streptavidin (N-Twin-Strep (N-TS)) tag sequences. Protein
360 expression was induced for 3 h at 37°C by the addition of 1 mM IPTG to *E. coli* BL21
361 cells (Wood, 1966). Cells expressing soluble MtNCC1$_{1\text{-}78}$ were disrupted in 100 mM Tris
362 (pH 8.0), 150 mM NaCl (buffer W) using a French press. Homogenates were centrifuged
363 at 54,000 g for 1 h. The protein was purified with a Strep-Tactin XT 4Flow high-capacity
364 column (IBA lifesciences) and stored in 10% glycerol in buffer W at -80°C. Protein
365 quantification was performed in accordance with Bradford assay (Bradford, 1976).

366

367 **Cu^+-binding affinity.**

368 MtNCC1$_{1\text{-}78}$·Cu^+ K_a value was obtained by using a competition assay with BCA
369 followed by colorimetric determination of the BCA_2·Cu^+ complex at 360 nm. MtNCC1$_{1\text{-}}$

370 $_{78}\cdot Cu^+$ K_a was determined by titrating with Cu^+ in a solution of 20 μM BCA, 100 μM
371 MtNCC1$_{1\text{-}78}$ in 50 mM HEPES (pH 7.5), 200 mM NaCl, and 200 μM ascorbate (buffer
372 H). The $BCA_2\cdot Cu^+$ molar extinction coefficient, ε_{360} = 20,600 cm^{-1} M^{-1}, was determined
373 by titrating μM Cu^+ with 0–10 μM BCA in buffer H. Free metal concentrations were
374 calculated from $K_{BCA} = [BCA_2\cdot Cu^+]/[BCA_{free}]^2[Cu^+_{free}]$, where K_{BCA} is the association
375 constant for $BCA_2\cdot Cu^+$ (4.60 x 10^{14} M^{-2}) (Yatsunyk and Rosenzweig, 2007; González-
376 Guerrero and Argüello, 2008). The MtNCC$_{1\text{-}78}\cdot Cu^+$ K_a value was calculated by using ν
377 $= [Cu^+_{free}]^n K_a/(1 + K_a [Cu^+_{free}]^n)$, where ν is the molar ratio of metal bound to protein and
378 *n* is the number of metal-binding sites. Reported errors for *Ka* and *n* are asymptotic
379 standard errors provided by the fitting software (Origin; OriginLab).
380
381 **GUS staining**
382 *MtNCC1* promoter (*MtNCC1p*; 2 kb upstream of the *MtNCC1* start codon) was
383 amplified using the primers indicated in Table S5, then cloned into pDONR207
384 (Invitrogen) and transferred to pGWB3 vector containing the *GUS* gene (Nakagawa et
385 al., 2007), using Gateway Cloning technology (Invitrogen). *M. truncatula* hairy-roots
386 transformation was carried out as described above. Transformed seedlings were planted
387 in sterile perlite pots and inoculated with *S. meliloti* 2011. GUS activity was measured in
388 nodules of 28 dpi plants as described (Vernoud et al., 2007).
389
390 **Immunolocalization**
391 A DNA fragment containing the full-length *MtNCC1* genomic region and the
392 *MtNCC1p* was cloned into the pGWB13 (Nakagawa et al., 2007) by Gateway technology
393 (Invitrogen). This vector fuses three HA epitopes in the C-terminus of the protein. *M.*
394 *truncatula* hairy-root transformation was carried out as described above (Boisson-Dernier
395 et al., 2001). Transformed seedlings were planted in sterile perlite pots and inoculated
396 with *S. meliloti* 2011 integrating the pHC60 vector that constitutively expresses GFP. 28
397 dpi nodules were collected and fixed in 4% (w/v) paraformaldehyde, 2.5% (w/v) sucrose
398 in phosphate-buffered saline (PBS) at 4°C overnight. Next day, nodules were washed in
399 PBS, and 100 μm sections were generated with a Vibratome 1000 plus (Vibratome).
400 Then, the sections were dehydrated using a methanol series (30%, 50%, 70% and 100%
401 [v/v] in PBS) for 5 min and then rehydrated. Cell walls were permeabilized with 4% (w/v)
402 cellulase in PBS for 1 h at room temperature and treated with 0.1% (v/v) Tween 20 in

403 PBS for 15 min. The sections were blocked with 5% (w/v) bovine serum albumin (BSA)
404 in PBS and incubated then with an anti-HA mouse monoclonal antibody (Sigma) for 2 h
405 at room temperature. After washing the primary antibody, the sections were incubated
406 with an Alexa594-conjugated anti-mouse rabbit monoclonal antibody (Sigma) for 1 h at
407 room temperature. After removing the unbound secondary antibody, DAPI (40,6-
408 diamidino-2-phenylindole) was used to stain the DNA. Images were acquired with a
409 confocal laser-scanning microscope (Leica SP8) using excitation lights at 488 nm for GFP
410 and at 561 nm for Alexa 594.
411 For gold-immunolocalization, 28 dpi nodules were collected and fixed in 1%
412 formaldehyde and 0.5% glutaraldehyde in 50 mM potassium phosphate (pH 7.4) for 2 h.
413 The fixation solution was renewed and incubated for an additional 1.5 h. Samples were
414 washed in 50 mM potassium phosphate (pH 7.4) 3 times during 30 min and 3 times for
415 10 min. Nodules were dehydrated by incubating with ethanol dilution series of 30%, 50%,
416 70%, and 90% during 10 min, 96% for 30 min, and 100% for 1 h. Samples were incubated
417 with a series of ethanol and LR-white resin (London Resin Company Ltd, UK) dilutions:
418 1:3 for 3 h, 1:1 overnight, and 3:1 for 3 h, and left in LR-white resin for 48 h. All
419 incubations were done at 4°C. Nodules were placed in gelatine capsules previously filled
420 with LR-white resin and polymerized at 60 °C for 24 h. Ultra-thin sections were cut at
421 Centro Nacional de Microscopia Electrónica (Universidad Complutense de Madrid,
422 Spain) with Reichert Ultracut S-ultramicrotome fitted with a diamond knife. The sections
423 were blocked in 2% bovine serum albumin (BSA) in PBS for 30 min. An anti-HA rabbit
424 monoclonal antibody (Sigma) was used (dilution 1:20 in PBS) as primary antibody. The
425 samples were washed 10 times in PBS for 2 min. As a secondary antibody, 1:150 dilution
426 in PBS of antirabbit goat antibody conjugated to a 15 nm gold particle (BBI solutions)
427 was used. Incubation was performed for 1 h. The sections were washed 10 times with
428 PBS for 2 min and 15 times with water for 2 min, stained with 2% uranyl acetate, and
429 visualized in a JEM 1400 electron microscope at 80 kV.
430
431 **Acetylene reduction assay**
432 Nitrogenase activity was determined by the acetylene reduction assay (Hardy et
433 al., 1968). Nitrogen fixation was analyzed in mutant and control plants at 28 dpi in 30-ml
434 vials fitted with rubber stoppers. Each tube contained one independently transformed
435 plant. Three ml of air inside the vial was replaced by 3 ml of acetylene and then they were
436 incubated at room temperature for 30 min. Gas samples (0.5 ml) were analyzed in a

437 Shimadzu GC-8A gas chromatograph fitted with a Porapak N column. The amount of
438 ethylene produced was determined by measuring the height of the ethylene peak relative
439 to the background. After measurements, nodules were collected from roots for weighing.
440
441 **Cytochrome oxidase activity**
442 Nodules from 28 dpi plants were collected and used for bacteroid isolation, as
443 described by (Brito et al., 1994) with modifications. Nodules from 50 plants (0.1-0.3 g
444 nodules) were pooled together and crushed with 33% (w/w) of polyvinylpyrrolidone and
445 1 ml of extraction buffer (38 mM K_2HPO_4, 24 mM KH_2PO_4, 2.4 mM $MgCl_2$). Three
446 consecutive centrifugations were performed with the supernatant of the previous one, two
447 at 1000 g (1 and 5 min) and a final one at 5000 g for 10 min. The final pellet was
448 resuspended in 500 µL of resuspension buffer (50 mM HEPES, 200 mM NaCl pH 7).
449 Cytochrome oxidase activity was determined by N,N,N',N'-tetramethyl-p-
450 phenylenediamine (TMPD) oxidation assay. The reaction was started by adding TMPD
451 to the bacteroid sample at a final concentration of 2.7 mM. To obtain the reaction kinetics,
452 each sample was measured at OD_{520} each 10 s for 3 min. To measure protein content and
453 to calculate specific activity, the bacteroid suspension was lysed in 10% SDS at 90°C for
454 5 min. The amount of protein was determined with the Pierce™ BCA Protein Assay Kit
455 (Thermo Scientific, Waltham, MA, USA).
456
457 **Metal content determination**
458 To determine metal content, Inductively Coupled Plasma-Mass Spectrometry
459 (ICP-MS) was performed for three independent sets of 28 dpi roots, shoots and nodules
460 pooled from ten plants. Elemental analysis with ICP-MS was carried out at the Unit of
461 Metal Analysis from the Scientific and Technology Centre, Universidad de Barcelona
462 (Spain). These samples were treated with HNO_3, H_2O_2 and HF in a Teflon reactor at 90°C.
463 The resulting homogenates were diluted with deionized water. Final volumes were
464 calculated by weight and weight: volume ratios. In parallel, samples were digested with
465 three blanks. Metal determination was carried out in an Agilent 7500cw with standard
466 instrument conditions. Calibration and internal standardization for obtaining the
467 calibration curve was done with five solutions prepared from certified NIST standards
468
469
470

471 **Metalloproteomics**

472 Metalloproteomic analyses were performed on 150 28 dpi nodules from wild type
473 or *ncc1* plants. Soluble and membrane proteins were extracted from the nodules as
474 described by Andresen et al. (2016). Afterwards, proteins were separated by size
475 exclusion chromatography coupled to ICP-sfMS as described (Küpper et al., 2019).
476 Briefly, two Superdex Increase 200 10 x 300 mm and one Superdex Increase 75 10 x 300
477 mm size exclusion columns were used to separate the nodule protein extracts in 150 mM
478 ammonium bicarbonate buffer with 0.2 mM DDM. Detection was achieved with a
479 customized sector field ICP-MS (Element XR-2 with jet interface and desolvating
480 injection, Thermo Scientific, Bremen Germany) and a diode array detector coupled to a
481 metal-free HPLC system (Azury system. Knauer, Germny). Metal-EDTA complexes in
482 the same buffer as the protein extracts were used to calibrate concentration determination.
483 A gel filtration calibration standard (Bio-rad with added PABA) was used to determine
484 size and molecular weight. Calibration of metal concentrations in the ICP-sfMS
485 chromatograms was performed as described in Küpper et al. (2019). Proteins were
486 identified in the Proteomic Unit of Universidad Complutense de Madrid (Spain).

487

488 **Proteomics**

489 Proteomic analyses were performed in the Proteomics Unit of Complutense
490 University of Madrid, a member of Proteored. Samples were liophylized and resuspended
491 in 100 µl of 25 mM ammonium bicarbonate buffer and quantified. Proteins were reduced
492 in 10 mM DTT at 56ºC for 60 min, and subsequently alkylated in 25 mM iodocetamide
493 for 60 min in darkness at room temperature. Samples were digested with Trypsine/LysC
494 protease mix (Pierce, ThermoFisher) at a 1:30 (w/w) ration overnight at 37ºC. Desalted
495 and concentrated peptides were liophylized and reconstituted in 15 µl 2% acetonitrile,
496 0.1% formic acid. One µg of peptides from each sample were analysed by liquid nano-
497 chromatography (Vanquish Neo, Thermo Scientific) coupled to a high-resolution mass
498 spectrometer (Q-Exactive HF (Thermo Scientific). The acquired MS/MS spectra were
499 analysed using Proteome Discoverer 3 (Thermo Scientific) using Mascot 2.8 search
500 engine and the databases SwissProt, *M. truncatula*, *S. meliloti* downloaded from Uniprot.
501 "Correctly" identified proteins are those that have a False Discovery Rate (FDR) below
502 1 % and at least on single peptide identified with high confidence (above 99 %).

503

504 **Pull-down assay**

505 28 grams of fresh *M. truncatula* R108 nodules (from approximately 2.500 plants)
506 were homogenized manually with a mortar and pestle. The homogenate was centrifuged
507 at 20,000 g 4°C for 30 min. To separate soluble from membrane proteins, the supernatant
508 ("cell free" extract) was centrifuged at 100,000 g 4°C for 1 h. The resulting supernatant
509 containing soluble proteins was loaded in Strep-Tactin XT 4Flow High-Capacity column
510 (IBA lifesciences) previously saturated with N-TS-MtNCC$_{1\text{-}78}$·Cu^{+}. Co-eluting proteins
511 were identified by liquid chromatography Mass Spectrometry (LC-MS/MS) at the
512 Proteomic Unit of the Universidad Complutense de Madrid (Spain).

513

514 **Bimolecular fluorescence complementation**

515 *MtNCC1$_{1\text{-}78}$* CDS was fused at the N-terminus to the N-fragment of YFP (Yellow
516 Fluorescence Protein) in the Gateway vector pNXGW (Kim et al., 2009). The CDS of
517 MtNCC1candidate interactors were fused to the C-fragment of CFP (Cyan Fluorescence
518 Protein) at both N and C-terminus in the Gateway vectors pCXGW and pXCGW (Kim et
519 al., 2009), respectively. Primers for cloning are indicated in Table S5. These constructs
520 were introduced into *A. tumefaciens* GV3101 (Deblaere et al., 1985).
521 *N. benthamiana* leaves were infiltrated as previously described (Senovilla et al., 2018).
522 Leaves were examined after 3 d by confocal laser-scanning microscopy (Zeiss LSM 880)
523 with excitation light of 488 nm for GFP.

524

525 **Statistical tests**

526 Data were analyzed using Student's unpaired t-test to calculate statistical
527 significance of observed differences. Test results with P-values lower than 0.05 were
528 considered as statistically significant.

529

530 **Data availability**

531 All the data included in this manuscript is available to interested researchers upon
532 request. Proteomics raw data have been deposited in Proteomics Identification Database
533 (PRIDE).

534

535 **FUNDING**

536 This research was funded by a Ministerio de Ciencia, Innovación y Universidades
537 grant (AGL2018-095996-B-100) to MG-G. CN-G is supported by Formación de Personal

de Investigación fellowship PRE2019-089164, and MR-S by Comunidad de Madrid contract from the Plan de Empleo Juvenil (PEJ-2020-TL-BIO-18547). Metalloproteomics studies were funded by the Ministry of Education, Youth and Sports of the Czech Republic with co-financing from the European Union (grant "KOROLID", CZ.02.1.01/0.0/0.0/15_003/0000336), the COST association (grant CA19116 “PLANTMETALS”) and the Czech Academy of Sciences (RVO: 60077344) to HK. Development of the *M. truncatula Tnt1* mutant population was, in part, funded by the National Science Foundation USA grant DBI-0703285.

AUTHOR CONTRIBUTIONS

CN-G performed most of the experimental work in this manuscript. JL-M contributed to the phenotype and confocal immunolocalization work and carried out the GUS, sequence comparison of *A. thaliana* and *M. truncatula* candidate Cu^{+}-chaperones, and the yeast complementation studies. HK and SNHB performed and analysed the metalloproteomic studies. MR-S contributed to plasmid generation and plant management. AP-L collaborated in the BiFC studies. JW and KSM produced and characterized the *M. truncatula Tnt1* collection. SB optimized $MtNCC1_{1\text{-}78}$ purification. JI, VE, and MG-G analysed data. VE and MG-G were responsible for overall research supervision and prepared the manuscript with input from all other authors.

ACKNOWLEDGEMENTS

The authors would like to thank Dr. Luis Fernández-Pacios (CBGP, UPM-INIA/CSIC, Spain) for his help with MtNCC1 modelling, and Dr. Luis Oñate (CBGP, UPM-INIA/CSIC, Spain) for giving us the plasmids used for the BiFC assays. We would also like to thank other members of laboratory 279 at Centro de Biotecnología y Genómica de Plantas (UPM-INIA/CSIC) for their support and feedback in preparing this manuscript.

569 **REFERENCES**

570 **Abreu, I., Saez, A., Castro-Rodríguez, R., Escudero, V., Rodríguez-Haas, B.,**
571 **Senovilla, M., Larue, C., Grolimund, D., Tejada-Jiménez, M., Imperial, J., et**
572 **al.** (2017). *Medicago truncatula* Zinc-Iron Permease6 provides zinc to rhizobia-
573 infected nodule cells. *Plant Cell Environ.* **40**:2706–2719.

574 **Andresen, E., Peiter, E., Küpper, H**. (2018). Trace metal metabolism in plants. *J Exp*
575 *Bot* **69:**909-954.

576 **Andresen, E., Kappel, S., Stärk, H.J., Riegger, U., Borovec, J., Mattusch, J., Heinz,**
577 **A., Schmelzer, C.E.H., Matoušková, Š., Dickinson, B., Küpper, H**. (2016).
578 Cadmium toxicity investigated at the physiological and biophysical levels under
579 environmentally relevant conditions using the aquatic model plant *Ceratophyllum*
580 *demersum* L. *New Phytol* **210**:1244-1258

581 **Attallah, C. v., Welchen, E., Martin, A. P., Spinelli, S. v., Bonnard, G., Palatnik, J.**
582 **F., and Gonzalez, D. H.** (2011). Plants contain two SCO proteins that are
583 differentially involved in cytochrome c oxidase function and copper and redox
584 homeostasis. *J Exp Bot* **62**:4281–4294.

585 **Blaby-Haas, C. E., Padilla-Benavides, T., Stübe, R., Argüello, J. M., and Merchant,**
586 **S. S.** (2014). Evolution of a plant-specific copper chaperone family for chloroplast
587 copper homeostasis. *Proc Nat Acad Sci USA* **111**:E5480–E5487.

588 **Boisson-Dernier, A., Chabaud, M., Garcia, F., Bécard, G., Rosenberg, C., and**
589 **Barker, D. G.** (2001). *Agrobacterium rhizogenes*-transformed roots of *Medicago*
590 *truncatula* for the study of nitrogen-fixing and endomycorrhizal symbiotic
591 associations. *Mol Plant Microbe Interact* **14**:695–700.

592 **Bradford, M. M.** (1976). A rapid and sensitive method for the quantitation of microgram
593 quantities of protein utilizing the principle of protein-dye binding. *Anal Biochem*
594 **7**:248–254.

595 **Brito, B., Palacios, J. M., Hidalgo, E., Imperial, J., and Ruiz-Argueso, T.** (1994a).
596 Nickel availability to pea (*Pisum sativum* L.) plants limits hydrogenase activity of
597 *Rhizobium leguminosarum* bv. *viciae* bacteroids by affecting the processing of the
598 hydrogenase structural subunits. *J Bacteriol* **176**:5297–5303.

599 **Burén, S., Jiménez-Vicente, E., Echavarri-Erasun, C., and Rubio, L. M.** (2020).
600 Biosynthesis of nitrogenase cofactors. *Chem Rev* **120**:4921-4968.

601 **Burkhead, J. L., Gogolin Reynolds, K. A., Abdel-Ghany, S. E., Cohu, C. M., and**
602 **Pilon, M.** (2009). Copper homeostasis. *New Phytol.* **182**:799–816.

603 **Castro-Rodríguez, R., Abreu, I., Reguera, M., Novoa-Aponte, L., Mijovilovich, A.,**
604 **Escudero, V., Jiménez-Pastor, F. J., Abadía, J., Wen, J., Mysore, K. S., et al.**
605 (2020). *The Medicago truncatula* Yellow Stripe1-Like3 gene is involved in vascular
606 delivery of transition metals to root nodules. *J Exp Bot* **71**:7257–7269.
607 **Chai, L.-X., Dong, K., Liu, S.-Y., Zhang, Z., Zhang, X.-P., Tong, X., Zhu, F.-F., Zou,**
608 **J.-Z., and Wang, X.-B.** (2020). A putative nuclear copper chaperone promotes plant
609 immunity in Arabidopsis. *J Exp Bot* **71**:6684–6696.
610 **Changella, A.** (2003). Molecular basis of metal-ion selectivity and zeptomolar sensitivity
611 by CueR. *Science* **301**:1383–1397.
612 **Cheng, H. P., and Walker, G. C.** (1998). Succinoglycan is required for initiation and
613 elongation of infection threads during nodulation of alfalfa by *Rhizobium meliloti*. *J*
614 *Bacteriol* **180**:5183–5191.
615 **Chu, C.-C., Lee, W.-C., Guo, W.-Y., Pan, S.-M., Chen, L.-J., Li, H., and Jinn, T.-L.**
616 (2005). A copper chaperone for superoxide dismutase that confers three types of
617 copper/zinc Superoxide dismutase activity in Arabidopsis. *Plant Physiol* **139**:425–
618 436.
619 **Deblaere, R., Bytebier, B., de Greve, H., Deboeck, F., Schell, J., van Montagu, M.,**
620 **and Leemans, J.** (1985). Efficient octopine Ti plasmid-derived vectors for
621 *Agrobacterium*-mediated gene transfer to plants. *Nucleic Acids Res* **13**:4777.
622 **Downie, J. A.** (2014). Legume nodulation. *Curr. Biol.* **24**:R184–R190.
623 **Escudero, V., Abreu, I., Tejada-Jiménez, M., Rosa-Núñez, E., Quintana, J., Prieto,**
624 **R. I., Larue, C., Wen, J., Villanova, J., Mysore, K. S., et al.** (2020a). *Medicago*
625 *truncatula* Ferroportin2 mediates iron import into nodule symbiosomes. *New*
626 *Phytologist* **228**:194–209.
627 **Escudero, V., Abreu, I., del Sastre, E., Tejada-Jiménez, M., Larue, C., Novoa-**
628 **Aponte, L., Castillo-González, J., Wen, J., Mysore, K. S., Abadía, J., et al.**
629 (2020b). Nicotianamine Synthase 2 Is required for symbiotic nitrogen fixation in
630 *Medicago truncatula* nodules. *Front. Plant Sci* **10**.
631 **Flis, P., Ouerdane, L., Grillet, L., Curie, C., Mari, S., and Lobinski, R.** (2016).
632 Inventory of metal complexes circulating in plant fluids: a reliable method based on
633 HPLC coupled with dual elemental and high-resolution molecular mass
634 spectrometric detection. *New Phytol.* **211**:1129–1141.
635 **Goldstein, S., Meyerstein, D., and Czapski, G.** (1993). The Fenton reagents. *Free Radic*
636 *Biol Med* **15**:435–445.

637 **González-Guerrero, M., and Argüello, J. M.** (2008). Mechanism of Cu^+-transporting
638 ATPases: Soluble Cu^+ chaperones directly transfer Cu^+ to transmembrane transport
639 sites. *Proc Natl Acad Sci U S A* **105**:5992-5997.
640 **González-Guerrero, M., Raimunda, D., Cheng, X., and Argüello, J. M.** (2010).
641 Distinct functional roles of homologous Cu^+ efflux ATPases in Pseudomonas
642 aeruginosa. *Mol Microbiol* **78**:1246-1258.
643 **González-Guerrero, M., Escudero, V., Sáez, Á., and Tejada-Jiménez, M.** (2016).
644 Transition metal transport in plants and associated endosymbionts. Arbuscular
645 mycorrhizal fungi and rhizobia. *Front. Plant Sci.* **7**:1088.
646 **Hardy, R. W. F., Holsten, R. D., Jackson, E. K., and Burns, R. C.** (1968). The
647 acetylene-ethylene assay for N_2 Fixation: Laboratory and field evaluation. *Plant*
648 *Physiol* **43**:1185–1207.
649 **Johnston, A. W., Yeoman, K. H., and Wexler, M.** (2001). Metals and the rhizobial-
650 legume symbiosis - uptake, utilization and signalling. *Adv. Microb. Physiol* **45**:113–
651 156.
652 **Kahn, D., David, M., Domergue, O., Daveran, M. L., Ghai, J., Hirsch, P. R., and**
653 **Batut, J.** (1989). *Rhizobium meliloti fixGHI* sequence predicts involvement of a
654 specific cation pump in symbiotic nitrogen fixation. *J Bacteriol* **171**:929–939.
655 **Kaur, A., Pati, P. K., Pati, A. M., and Nagpal, A. K.** (2017). In-silico analysis of cis-
656 acting regulatory elements of pathogenesis-related proteins of *Arabidopsis thaliana*
657 and *Oryza sativa*. *PLoS One* **12**:e0184523.
658 **Kim, J. G., Li, X., Roden, J. A., Taylor, K. W., Aakre, C. D., Su, B., Lalonde, S.,**
659 **Kirik, A., Chen, Y., Baranage, G., et al.** (2009). *Xanthomonas* T3S effector XopN
660 suppresses PAMP-triggered immunity and interacts with a tomato atypical
661 Receptor-Like Kinase and TFT1. *Plant Cell* **21**:1305-1323.
662 **Kryvoruchko, I. S., Routray, P., Sinharoy, S., Torres-Jerez, I., Tejada-Jiménez, M.,**
663 **Finney, L. A., Nakashima, J., Pislariu, C. I., Benedito, V. A., González-**
664 **Guerrero, M., et al.** (2018). An iron-activated citrate transporter, MtMATE67, is
665 required for symbiotic nitrogen fixation. *Plant Physiol* **176**:2315–2329.
666 **Küpper, H., Küpper, F., Spiller, M.** (1996). Environmental relevance of heavy metal
667 substituted chlorophylls using the example of submersed water plants. *J Exp Bot*
668 **47:**259-266.

669 **Küpper, H., Šetlík, I., Spiller, M., Küpper F.C., Prášil, O.** (2002). Heavy metal-
670 induced inhibition of photosynthesis: targets of in vivo heavy metal chlorophyll
671 formation. *J Phycol* **38:**429-441.
672 **Küpper, H., Andresen, E**. (2016). Mechanisms of metal toxicity in plants. *Metallomics*
673 **8**:269-285.
674 **Küpper, H., Bokhari, S. N. H., Jaime-Pérez, N., Lyubenova, L., Ashraf, N., and**
675 **Andresen, E.** (2019). Ultratrace metal speciation analysis by coupling of sector-
676 field ICP-MS to high-resolution size exclusion and reversed-phase liquid
677 chromatography. *Anal Chem* **91**:10961–10969.
678 **Li, L., and Kaplan, J.** (2001). The yeast gene MSC2, a member of the Cation Diffusion
679 Facilitator family, affects the cellular distribution of zinc. *J Biol Chem* **276**:5036–
680 5043.
681 **Lin, S.-J., Pufahl, R. A., Dancis, A., O'Halloran, T. v, and Culotta, V. C.** (1997). A
682 role for the *Saccharomyces cerevisiae* ATX1 gene in copper trafficking and iron
683 transport. *J Biol Chem* **272**:9215–9220.
684 **Liu, M., Saha, N., Gajan, A., Saadat, N., Gupta, S. v., and Pile, L. A.** (2020). A
685 complex interplay between SAM synthetase and the epigenetic regulator SIN3
686 controls metabolism and transcription. *J Biol Chem* **295**:375–389.
687 **Macomber, L., and Imlay, J. A.** (2009). The iron-sulfur clusters of dehydratases are
688 primary intracellular targets of copper toxicity. *Proc. Natl. Acad. Sci. U S A*
689 **106**:8344–8349.
690 **Maróti, G., Downie, J. A., and Kondorosi, E.** (2015). Plant cysteine-rich peptides that
691 inhibit pathogen growth and control rhizobial differentiation in legume nodules.
692 *Curr Opin Plant Biol* **26**:57–63.
693 **Marschner, H., and Marschner, P.** (2011). *Marschner's Mineral Nutrition of Higher*
694 *Plants*. Elsevier Science.
695 **Merkle, T.** (2011). Nucleo-cytoplasmic transport of proteins and RNA in plants. *Plant*
696 *Cell Rep* **30**:153–176.
697 **Mira, H., Martínez-García, F., and Peñarrubia, L.** (2001). Evidence for the plant-
698 specific intercellular transport of the Arabidopsis copper chaperone CCH. *Plant J.*
699 **25**:521–528.
700 **Nakagawa, T., Kurose, T., Hino, T., Tanaka, K., Kawamukai, M., Niwa, Y.,**
701 **Toyooka, K., Matsuoka, K., Jinbo, T., and Kimura, T.** (2007). Development of

series of gateway binary vectors, pGWBs, for realizing efficient construction of fusion genes for plant transformation. *J Biosci Bioeng* **104**:34–41.

O'Hara, G. W. (2001). Nutritional constraints on root nodule bacteria affecting symbiotic nitrogen fixation: a review. *Aust. J. Exp. Agr.* **41**:417–433.

Palumaa, P., Kangur, L., Voronova, A., and Sillard, R. (2004). Metal-binding mechanism of Cox17, a copper chaperone for cytochrome c oxidase. *Biochem J* **382**:307–314.

Preisig, O., Zufferey, R., Thony-Meyer, L., Appleby, C. A., and Hennecke, H. (1996). A high-affinity cbb3-type cytochrome oxidase terminates the symbiosis- specific respiratory chain of *Bradyrhizobium japonicum*. *J. Bacteriol.* **178**:1532–1538.

Rae, T. D., Schmidt, P. J., Pufahl, R. A., Culotta, V. C., and v. O'Halloran, T. (1999). Undetectable intracellular free copper: The requirement of a copper chaperone for superoxide dismutase. *Science* **284**:805–808.

Robinson, N. J., and Winge, D. R. (2010). Copper metallochaperones. *Annu. Rev. Biochem.* **79**:537–562.

Schiestl, R. H., and Gietz, R. D. (1989). High efficiency transformation of intact yeast cells using single stranded nucleic acids as a carrier. *Curr Genet* **16**:339–346.

Senovilla, M., Castro-Rodríguez, R., Abreu, I., Escudero, V., Kryvoruchko, I., Udvardi, M. K., Imperial, J., and González-Guerrero, M. (2018). *Medicago truncatula* copper transporter 1 (MtCOPT1) delivers copper for symbiotic nitrogen fixation. *New Phytologist* **218**:696–709.

Sherman, Fred., Fink, G. R., Hicks, J. B., and Cold Spring Harbor Laboratory. (1983). Methods in yeast genetics. Cold Spring Harbour Lab.

Shin, L.-J., Lo, J.-C., and Yeh, K.-C. (2012). Copper chaperone antioxidant protein1 is essential for copper homeostasis. *Plant Physiol* **159**:1099–1110.

Tejada-Jiménez, M., Castro-Rodríguez, R., Kryvoruchko, I., Mercedes Lucas, M., Udvardi, M., Imperial, J., and González-Guerrero, M. (2015). *Medicago truncatula* Natural Resistance-Associated Macrophage Protein1 is required for iron uptake by rhizobia-infected nodule cells. *Plant Physiol* **168**:258–272.

Tejada-Jiménez, M., Gil-Diez, P., Leon-Mediavilla, J., Wen, J., Mysore, K. S., Imperial, J., and Gonzalez-Guerrero, M. (2017). *Medicago truncatula* Molybdate Transporter type 1 (MOT1.3) is a plasma membrane molybdenum transporter required for nitrogenase activity in root nodules under molybdenum deficiency. *New Phytol* **216**:1223–1235.

736 **Udvardi, M., and Poole, P. S.** (2013). Transport and metabolism in legume-rhizobia
737 symbioses. *Annu Rev Plant Biol* **64**:781–805.
738 **Vasse, J., de Billy, F., Camut, S., and Truchet, G.** (1990). Correlation between
739 ultrastructural differentiation of bacteroids and nitrogen fixation in alfalfa nodules.
740 *J. Bacteriol.* **172**:4295–4306.
741 **Vernoud, V., Journet, E. P., and Barker, D. G.** (2007). MtENOD20, a Nod factor-
742 inducible molecular marker for root cortical cell activation. *Mol Plant Microbe*
743 *Interact* **12**:604–614.
744 **Wong, P. C., Waggoner, D., Subramaniam, J. R., Tessarollo, L., Bartnikas, T. B.,**
745 **Culotta, V. C., Price, D. L., Rothstein, J., and Gitlin, J. D.** (2000). Copper
746 chaperone for superoxide dismutase is essential to activate mammalian Cu/Zn
747 superoxide dismutase. *Proc Nat Acad Sci USA* **97**:2886–2891.
748 **Wood, W. B.** (1966). Host specificity of DNA produced by Escherichia coli: bacterial
749 mutations affecting the restriction and modification of DNA. *J Mol Biol* **16**:118–
750 133.
751 **Xiao, T. T., Schilderink, S., Moling, S., Deinum, E. E., Kondorosi, E., Franssen, H.,**
752 **Kulikova, O., Niebel, A., and Bisseling, T.** (2014). Fate map of *Medicago*
753 *truncatula* root nodules. *Development* **141**:3517–3528.
754 **Yatsunyk, L. A., and Rosenzweig, A. C.** (2007). Cu(I) binding and transfer by the N
755 terminus of the Wilson disease protein. *J Biol Chem* **282**:8622–8631.
756
757
758
759
760

761 **FIGURE LEGENDS**

762 **Figure 1. MtNCC1 is a nodule-specific Cu^+-chaperone.** A, *MtNCC1* expression in *S.*
763 *meliloti*-inoculated (roots, shoots, and nodules) and non-inoculated (roots and shoots)
764 plants relative to standard gene *Ubiquitin carboxyl-terminal hydrolase.* Data are the mean
765 ± SE of three independent experiments with five pooled plants. B, Predicted structure of
766 MtNCC1. The classical Atx1-like domain is indicated in pink, with the two conserved
767 Cu^+-binding cysteines (C22 and 25). The glutamate-rich region in the C-terminal domain
768 is indicated with wireframes. C, Parental strain BY4741 was transformed with empty
769 pDR196 vector, while the Δatx1 mutant NCC1 was transformed with empty pDR196 or
770 containing MtNCC1 or $MtNCC1_{1-78}$. D, Cu^+ binding to $MtNCC1_{1-78}$ determined in
771 competition assays with BCA. The data were fit using n = 1.03 ± 0.04 Cu^+ per protein
772 and $K_a = 2{,}45 \cdot 10^{-12} \pm 3.44 \cdot 10^{-13}$ M^{-1}. Data are the mean ± SE (n = 3).
773

774 **Figure 2. Localization of MtNCC1 in *M. truncatula* nodules.** A, GUS staining of 28
775 dpi nodules expressing the *gus* gene under the control of the *MtNCC1* promoter region.
776 Left panel shows the whole nodule and right panel shows a longitudinal section with the
777 different developmental zones indicated. Bars = 400 µm. B, *MtNCC1* expression in the
778 different nodule zones as indicated in the Symbimics database
779 (http://ia.nt.toulouse.inra.fr/symbimics/). ZI: zone I; ZIIp: zone II proximal; ZIId: zone
780 II distal; IZ: interzone; ZII: zone III. C, Longitudinal section of 28 dpi *M. truncula*
781 nodules expressing *MtNCC1* fused to three HA domains driven by its own promoter. HA-
782 tagged proteins were detected with using an Alexa594 conjugated antibody (red, left
783 panel). Nodules were colonized by a GFP-expressing *S. meliloti* (green, central panel).
784 DNA was stained with DAPI (blue) and overlaid with the previous two channels and the
785 transillumination signal (right panel). Bars = 100 µm. D, Closer view of rhizobia-infected
786 cell in zone II. Bars = 10 µm. E, Immunolocalization of MtNCC1-HA in 28 dpi nodules
787 using gold-conjugated antibodies and electron transmission microscopy. Gold particles
788 are indicated by arrows and asterisks represent bacteroids. PM indicates Plasma
789 membrane, and Mit refers to mitochondria. Bars = 1µm.
790

791 **Figure 3. MtNCC1 is required for nitrogen fixation**. A, Amplification of *MtNCC1*
792 transcript by RT-PCR in 28 dpi nodules of wild type and *ncc1* mutants. *MtUb1* (*Ubiquitin*
793 *carboxyl-terminal hydrolase 1*) was used as a constitutive gene. B, Growth of

794 representative plants of wild type (WT), *ncc1* mutant and *ncc1* mutants transformed with
795 *MtNCC1* regulated by its own promoter. Bar = 1cm. C, Fresh weight of shoots and roots
796 of WT, *ncc1* and *ncc1* transformed with *MtNCC1* regulated by its own promoter. Data
797 are the mean ± SE (n = 15). D, Acetylene reduction assay in 28 dpi nodules from WT,
798 *ncc1* mutants and *ncc1* transformed with *MtNCC1* regulated by its own promoter. Data
799 are the mean ± SE (n = 7-13). E, Cytochrome oxidase (COX) activity in bacteroids
800 isolated from 28 dpi nodules of WT and *ncc1* mutant plants. Data are the mean ± SE of
801 at least three sets of 35-40 pooled plants each. Student's *t*-test was used for statistical
802 analysis (* = P≤ 0.05).
803
804 **Figure 4. Copper supplementation complements the *ncc1* phenotype.** A, Growth of
805 representative plants of wild type (WT) and *ncc1* mutant watered with standard copper
806 concentrations (0.16 μM) and copper excess (1.6 μM). Bar = 1cm. B, Fresh weight of
807 shoots and roots of WT and *ncc1* mutant watered with standard copper concentrations
808 (0.16 μM) and copper excess (1.6 μM). Data are the mean ± SE (n = 16-23). C, Acetylene
809 reduction assay in 28 dpi nodules from WT and *ncc1* mutant watered with standard copper
810 concentrations (0.16 μM) and copper excess (1.6 μM). Data are the mean ± SE (n = 16-
811 23). All comparison were done to WT samples using Student's *t*-test (* = P≤ 0.05).
812
813 **Figure 5. Mutation of *MtNCC1* does not alter the nodule metallome.** A, Copper
814 content in 28 dpi shoots, roots and nodules of wild type (WT) and *ncc1* plants. Data are
815 the mean ± SE of three sets of ten pooled plants. B, Iron content in 28 dpi shoots, roots
816 and nodules of wild type (WT) and *ncc1* plants. Data are the mean ± SE of three sets of
817 ten pooled plants.
818
819 **Figure 6. Mutation of *MtNCC1* alters the nodule copper-proteome.** A,
820 Metalloproteomics by HPLC-ICPsfMS. The normalized chromatograms show copper
821 content in two independent biological replicates of 28 dpi WT and *ncc1* nodules.
822 Fractions subjected to proteomic analyses are boxed and indicated as F1 and F2. B and
823 C, Comparison of the most important element chromatograms and UV/VIS absorption
824 DAD in the chromatogram region where the biggest differences between the mutant had
825 been seen in the copper chromatogram. B, replicate 1 of the WT, C, replicate 1 of the
826 *ncc1* mutant.

827 **Figure 7**. **Bimolecular Fluorescent Complementation assays of MtNCC1$_{1-78}$**
828 **interactions.** Transient co-expression of MtNCC1$_{1-78}$ in pNXGW and candidate proteins
829 thioredoxin-dependent peroxiredoxin (A) and SAM synthase (B) in pCXGW, putative
830 universal stress protein (C) and pathogenesis-related protein (D) in pXCGW, in *N.*
831 *benthamiana* leaf cells 3 days-post-agroinfiltration. Left panel corresponds to the
832 fluorescent signal of MtNCC1$_{1-78}$ and corresponding interactor (green); central panel,
833 transillumination; right panel, overlaid fluorescent image and transillumination images.
834 Bars = 20 μm.
835
836
837
838
839
840
841

842 **TABLES**

843 **Table 1**. Top ten most abundant proteins detected in wild type replicates and not in *ncc1*
844 replicates in Fractions 1 or 2 of the metalloproteomic analyses of nodule soluble proteins.

Uniprot Accesion	Organism	Description	Fraction
Q4H1G3	*M. truncatula*	S-adenosylmethionine synthase	1
A0A072U7P3	*M. truncatula*	Heat shock cognate 70 kDa protein	1
P47923	*M. truncatula*	Nucleoside diphosphate kinase 2	1
Q1SL05	*M. truncatula*	Putative small GTPase superfamily, P-loop containing nucleoside triphosphate hydrolase	2
G7IEZ9	*M. truncatula*	Chalcone-flavonone isomerase family protein 2	1
Q92M81	*S. meliloti*	Glyceraldehyde-3-phosphate dehydrogenase	1
A0A072UDY2	*M. truncatula*	Presequence protease	1
Q92SW9	*S. meliloti*	Recombination protein Rec	2
Q92RK3	*S. meliloti*	4-phospho-D-erythronate dehydrogenase	1
Q92RH2	*S. meliloti*	3,4-dihydroxy-2-butanone 4-phosphate synthase	1

845

Figure 1

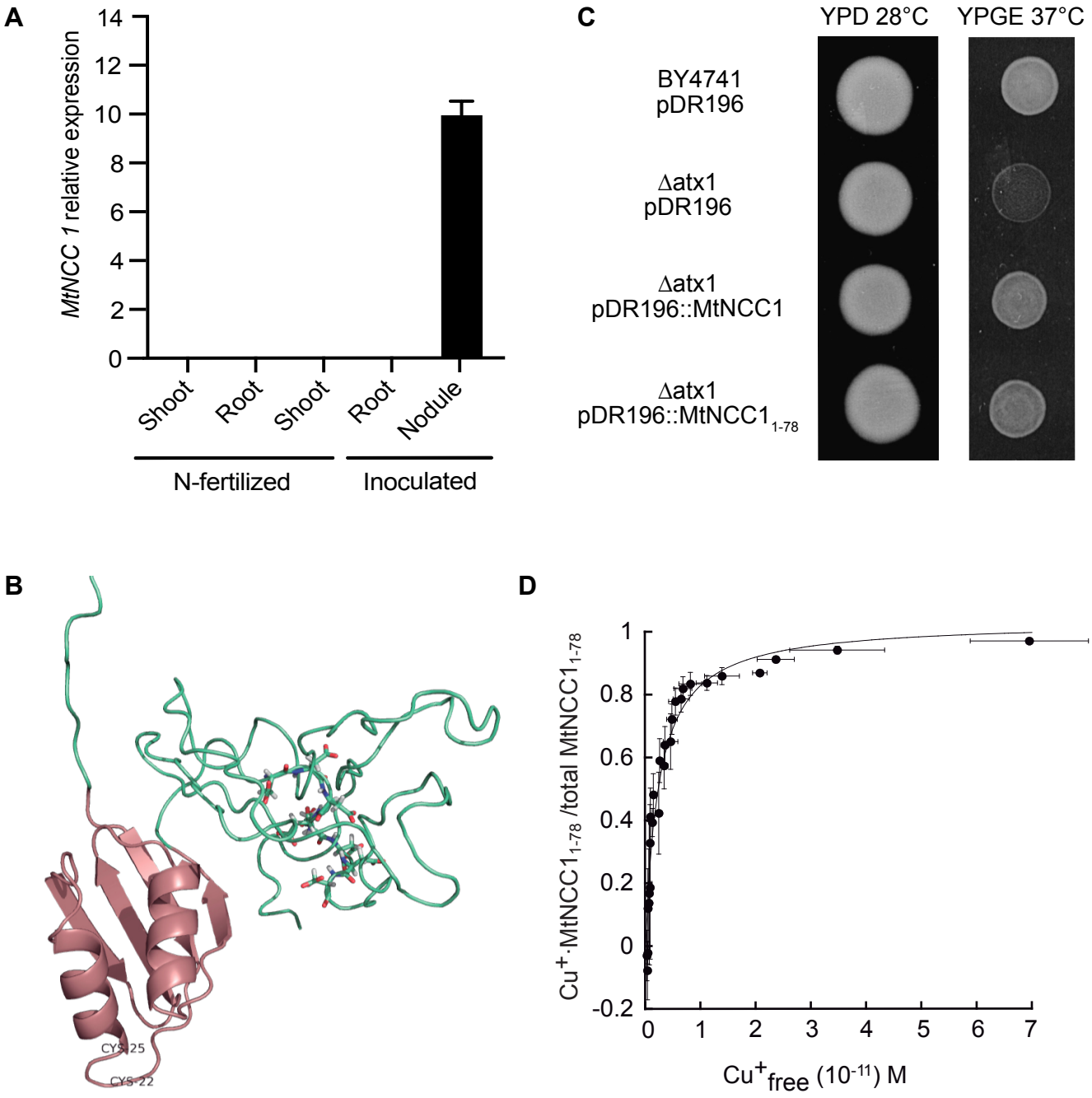

Figure 1. MtNCC1 is a nodule-specific Cu^{+}-chaperone. A, *MtNCC1* expression in *S. meliloti*-inoculated (roots, shoots, and nodules) and non-inoculated (roots and shoots) plants relative to standard gene U*biquitin carboxyl-terminal hydrolase*. Data are the mean ± SE of three independent experiments with five pooled plants. B, Predicted structure of MtNCC1. The classical Atx1-like domain is indicated in pink, with the two conserved Cu+-binding cysteines (C22 and 25). The glutamate-rich region in the C-terminal domain is indicated with wireframes. C, Parental strain BY4741 was transformed with empty pDR196 vector, while the Δatx1 mutant NCC1 was transformed with empty pDR196 or containing MtNCC1 or MtNCC11-78. D, Cu^{+} binding to $MtNCC1_{1-78}$ determined in competition assays with BCA. The data were fit using n = 1.03 ± 0.04 Cu^{+} per protein and K_a = $2{,}45 \cdot 10^{-12} \pm 3.44 \cdot 10^{-13}$ M^{-1}. Data are the mean ± SE (n = 3).

Figure 2

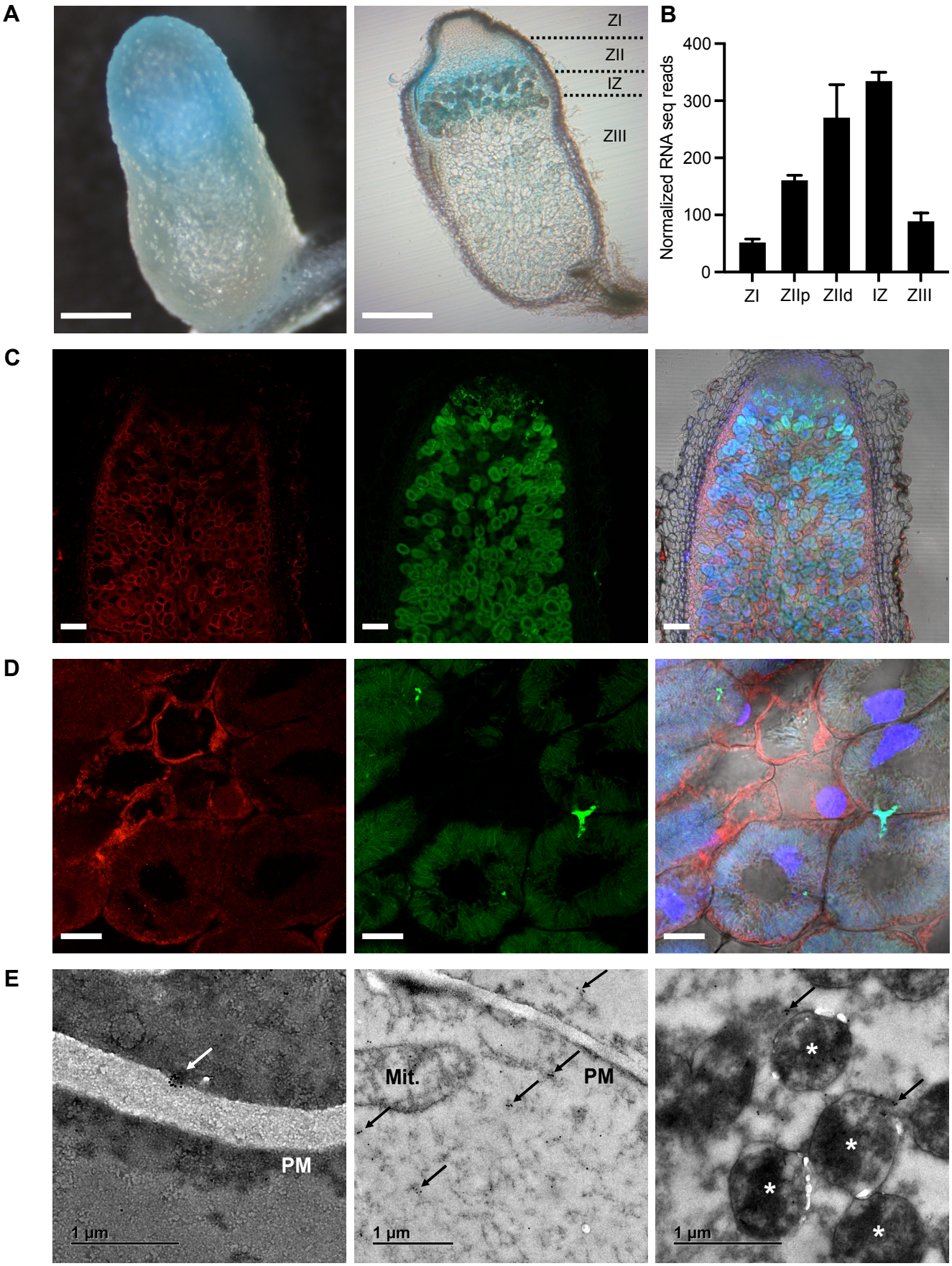
A
ZI
ZII
IZ
ZIII
B
Normalized RNA seq reads
400
300
200
100
0
ZI
ZIIp
ZIId
IZ
ZIII
C
D
E
PM
1 µm
Mit.
PM
1 µm
1 µm

Figure 2. Localization of MtNCC1 in *M. truncatula* nodules. A, GUS staining of 28 dpi nodules expressing the *gus* gene under the control of the *MtNCC1* promoter region. Left panel shows the whole nodule and right panel shows a longitudinal section with the different developmental zones indicated. Bars = 400 μm. B, *MtNCC1* expression in the different nodule zones as indicated in the Symbimics database (http://ia.nt.toulouse.inra.fr/symbimics/). ZI: zone I; ZIIp: zone II proximal; ZIId: zone II distal; IZ: interzone; ZII: zone III. C, Longitudinal section of 28 dpi *M. truncula* nodules expressing *MtNCC1* fused to three HA domains driven by its own promoter. HA-tagged proteins were detected with using an Alexa594 conjugated antibody (red, left panel). Nodules were colonized by a GFP-expressing *S. meliloti* (green, central panel). DNA was stained with DAPI (blue) and overlaid with the previous two channels and the transillumination signal (right panel). Bars = 100 μm. D, Closer view of rhizobia-infected cell in zone II. Bars = 10 μm. E, Immunolocalization of MtNCC1-HA in 28 dpi nodules using gold-conjugated antibodies and electron transmission microscopy. Gold particles are indicated by arrows and asterisks represent bacteroids. PM indicates Plasma membrane, and Mit refers to mitochondria. Bars = 1 μm.

Figure 3

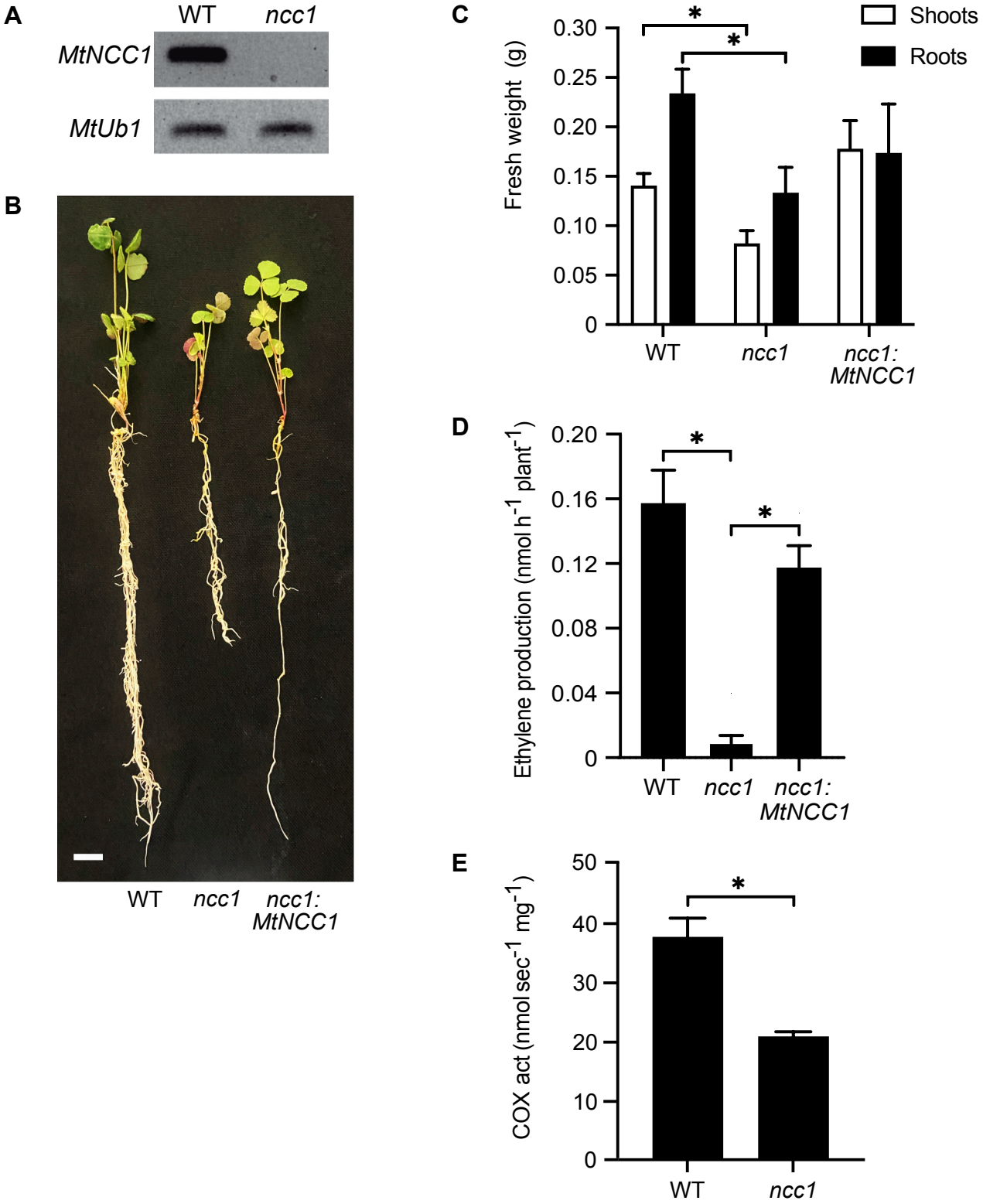

Figure 3. MtNCC1 is required for nitrogen fixation. A, Amplification of *MtNCC1* transcript by RT-PCR in 28 dpi nodules of wild type and *ncc1* mutants. *MtUb1* (*Ubiquitin carboxyl-terminal hydrolase 1*) was used as a constitutive gene. B, Growth of representative plants of wild type (WT), *ncc1* mutant and *ncc1* mutants transformed with *MtNCC1* regulated by its own promoter. Bar = 1cm. C, Fresh weight of shoots and roots of WT, *ncc1* and *ncc1* transformed with *MtNCC1* regulated by its own promoter. Data are the mean ± SE (n = 15). D, Acetylene reduction assay in 28 dpi nodules from WT, *ncc1* mutants and *ncc1* transformed with *MtNCC1* regulated by its own promoter. Data are the mean ± SE (n = 7-13). E, Cytochrome oxidase (COX) activity in bacteroids isolated from 28 dpi nodules of WT and *ncc1* mutant plants. Data are the mean ± SE of at least three sets of 35-40 pooled plants each. Student's *t*-test was used for statistical analysis (* = P< 0.05).

Figure 4

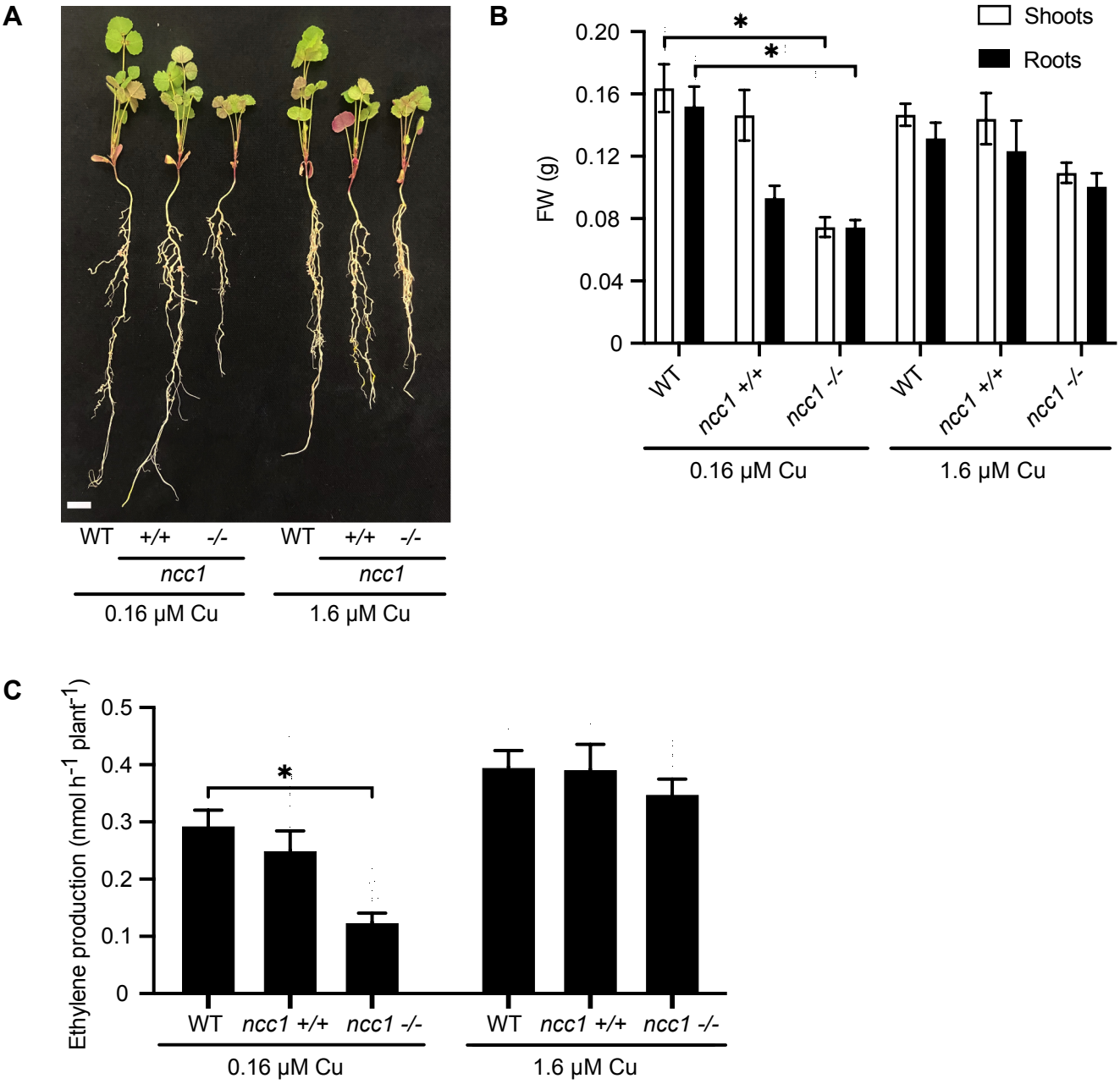

Figure 4. Copper supplementation complements the *ncc1* phenotype. A, Growth of representative plants of wild type (WT) and *ncc1* mutant watered with standard copper concentrations (0.16 µM) and copper excess (1.6 µM). Bar = 1cm. B, Fresh weight of shoots and roots of WT and *ncc1* mutant watered with standard copper concentrations (0.16 µM) and copper excess (1.6 µM). Data are the mean ± SE (n = 16-23). C, Acetylene reduction assay in 28 dpi nodules from WT and *ncc1* mutant watered with standard copper concentrations (0.16 µM) and copper excess (1.6 µM). Data are the mean ± SE (n = 16-23). All comparison were done to WT samples using Student's *t*-test (* = P< 0.05).

Figure 5

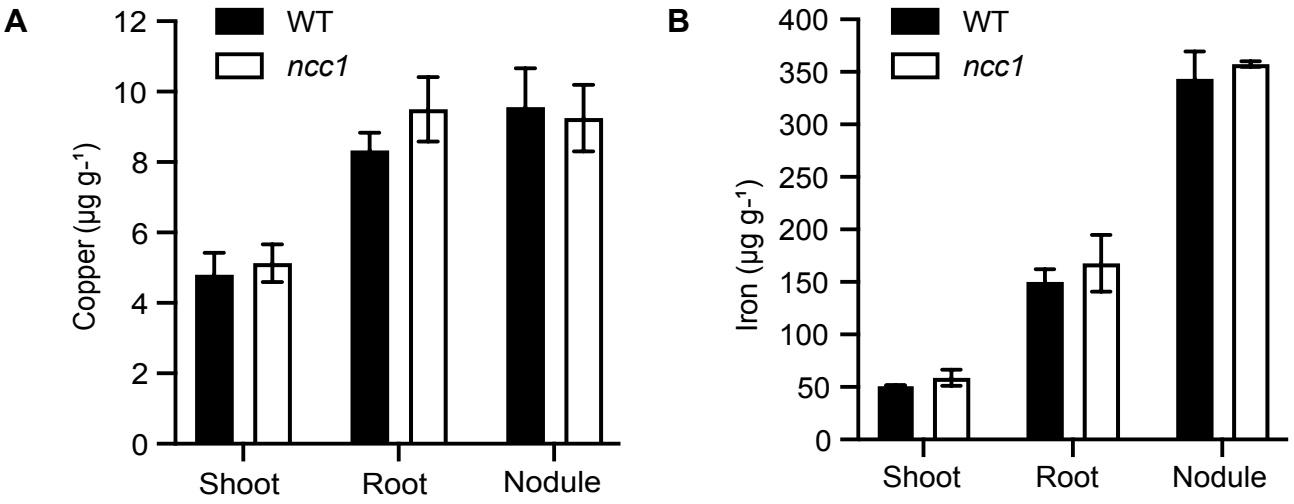

Figure 5. Mutation of *MtNCC1* does not alter the nodule metallome. A, Copper content in 28 dpi shoots, roots and nodules of wild type (WT) and *ncc1* plants. Data are the mean + SE of three sets of ten pooled plants. B, Iron content in 28 dpi shoots, roots and nodules of wild type (WT) and *ncc1* plants. Data are the mean + SE of three sets of ten pooled plants.

Figure 6

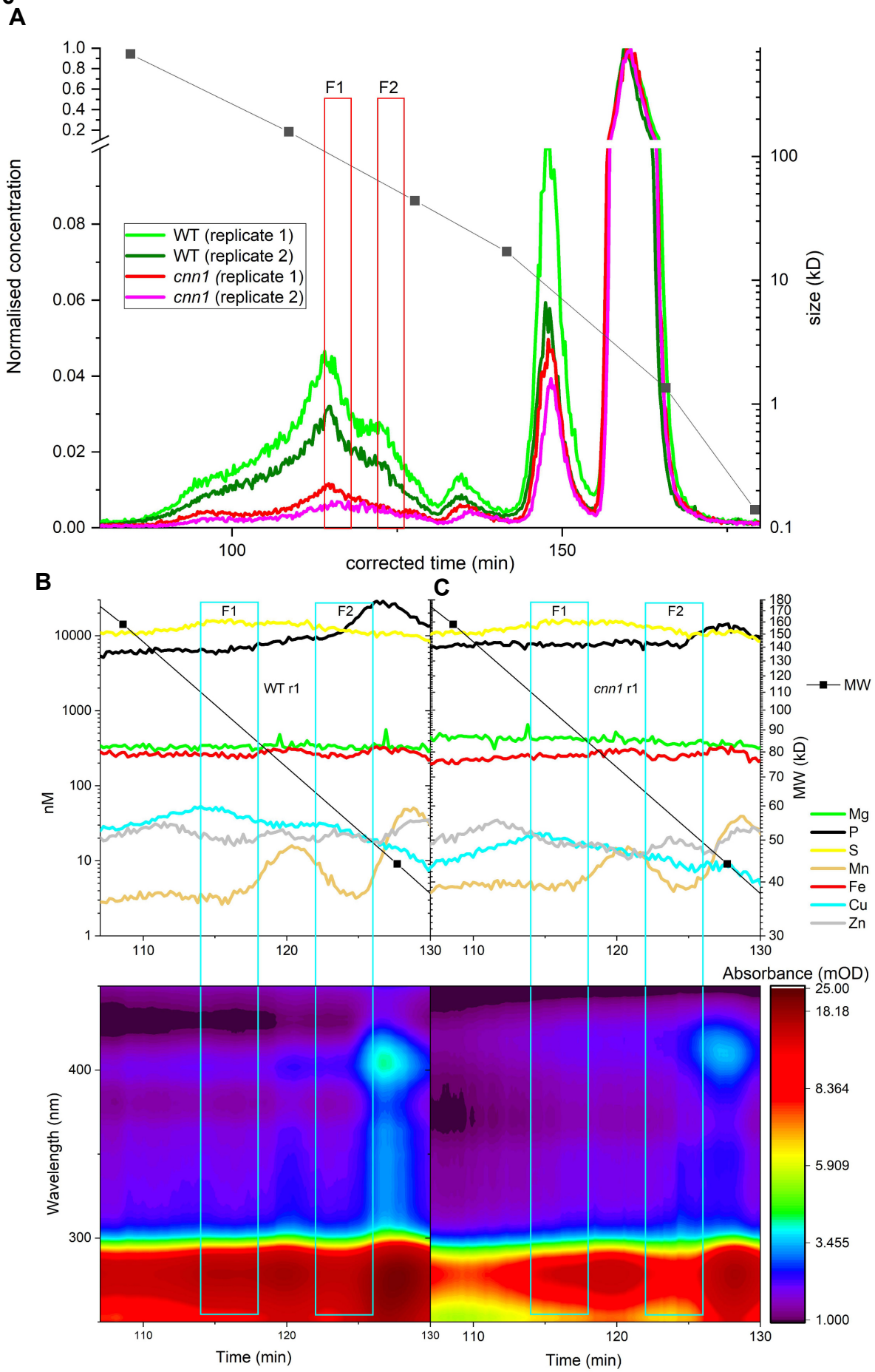

Figure 6. Mutation of MtNCC1 alters the nodule copper-proteome. A, Metalloproteomics by HPLC-ICPsfMS. The normalized chromatograms show copper content in two independent biological replicates of 28 dpi WT and *ncc1* nodules. Fractions subjected to proteomic analyses are boxed and indicated as F1 and F2. B and C, Comparison of the most important element chromatograms and UV/VIS absorption DAD in the chromatogram region where the biggest differences between the mutant had been seen in the copper chromatogram. B, replicate 1 of the WT, C, replicate 1 of the *ncc1* mutant.

Figure 7

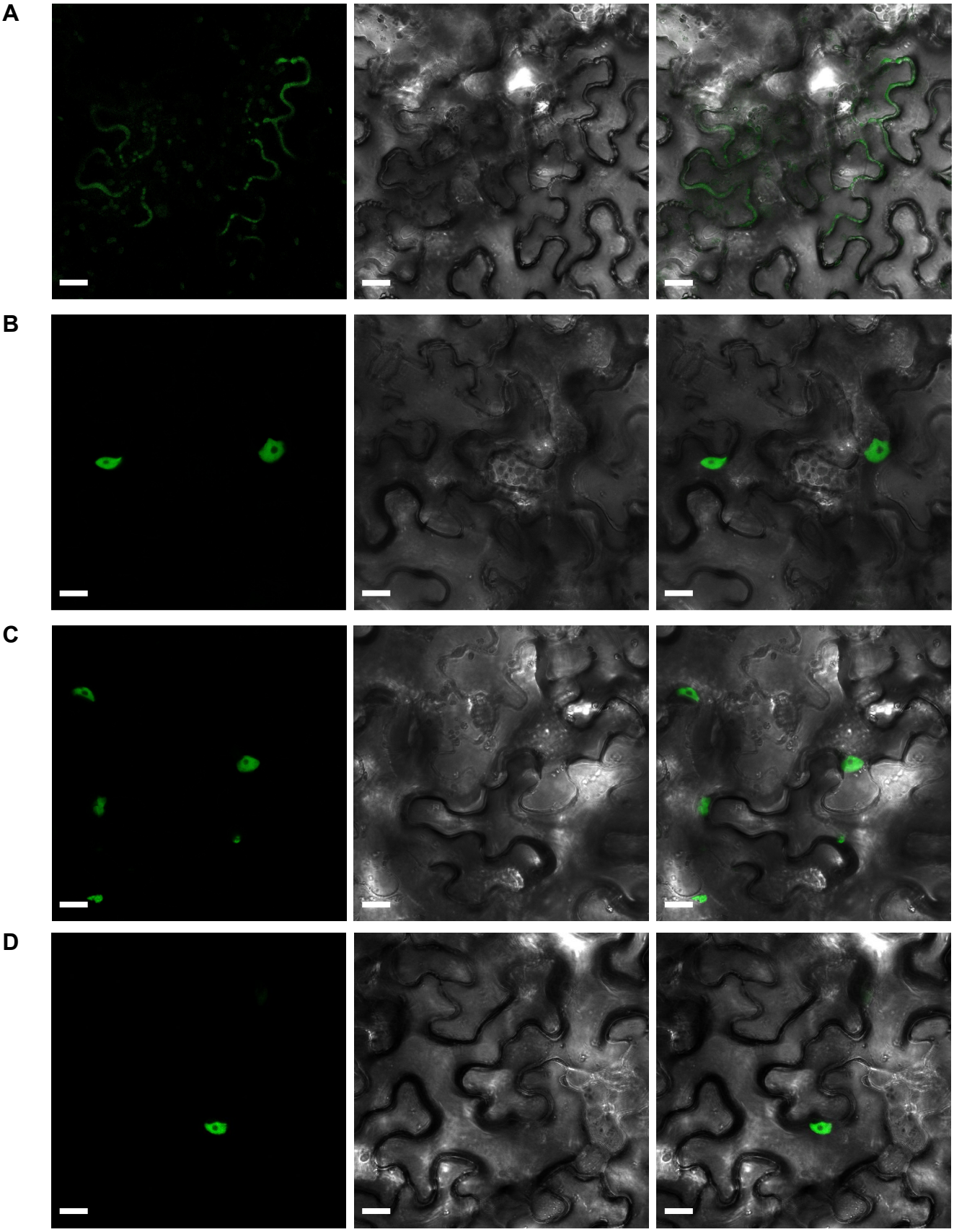

Figure 7. Bimolecular Fluorescent Complementation assays of MtNCC1$_{1\text{-}78}$ interactions. Transient co-expression of MtNCC1$_{1\text{-}78}$ in pNXGW and candidate proteins thioredoxin-dependent peroxiredoxin (A) and SAM synthase (B) in pCXGW, putative universal stress protein (C) and pathogenesis-related protein (D) in pXCGW, in *N. benthamiana* leaf cells 3 days-post-agroinfiltration. Left panel corresponds to the fluorescent signal of MtNCC1$_{1\text{-}78}$ and corresponding interactor (green); central panel, transillumination; right panel, overlaid fluorescent image and transillumination images. Bars = 20 µm.